Electronic Supplementary Information

Vacancy-Rich Graphene Supported Electrocatalysts Synthesized by Radio-Frequency Plasma for Oxygen Evolution Reaction

Wenkai He, Shilin Wu,* Zhaotian Zhang and Qing Yang*

State Key Laboratory of Power Transmission Equipment and System Security and New Technology, Chongqing University, Chongqing 400044, China

E-mail: wushilin@cqu.edu.cn and yangqing@cqu.edu.cn

Experimental Section

1. Preparation of Co supported on graphene oxide samples

For each sample, 50 mg of graphene oxide (GO, purity 99%, Shanghai Maclin Biochemical Technology Co., LTD) was added to 20 mL of deionized water to configure the GO suspension and ultrasonically dispersed for 30 min. Then 291 mg of cobalt nitrate hexahydrate (1 mM $Co(NO_3)_2 \cdot 6H_2O$, purity 99.99%, Shanghai Maclin Biochemical Technology Co., LTD) was mixed with 304.5 mg of thiourea (4 mMCH_4N_2S, Shanghai Maclin Biochemical Technology Co., LTD) in 2.5 mL of deionized water and sonicated for 30 min. Thereafter, the above two solutions were mixed and then sonicated for 30 min and the mixture was dried overnight.

To further investigate different types of vacancy defect structures (oxygen vacancy), 240 mg urea (4 mM CH_4N_2O, Shanghai Maclin Biochemical Technology Co., LTD) was used to replace thiourea in the previous experiment, and the samples configured according to the above process were used as auxiliary controls.

2. Experiment of RF plasma treatment of samples

The experimental system for RF plasma-assisted treatment of materials used in this study is shown in Fig. S1. The system was composed of an RF power generator (13.56 MHz, Beijing Gmpower Tech Co., Ltd), a matching network, and a vacuum system. A piece of copper sheet wrapped around the quartz tube was used as an electrode and connected to the RF power supply. Hydrogen gas (H_2, 99.999% purity,

produced by a commercial hydrogen generator.), Argon gas (Ar, 99.999% purity) and Ar/H_2 gas mixture (1:1 volume ratio) were used to generate plasma, separately. Typically, 100 mg of the samples were placed on a quartz boat. The reaction chamber was evacuated for 2 min. Then same gas as that used for the generation of plasma was introduced for 5 min at a flow rate of 100 sccm to purge the residual air. Thereafter, RF power was set to 80 W, and plasma was generated After 30 min of reaction, the temperature inside the chamber was found to be around 200 °C. Each sample was treated for 30 min and six groups of OER catalysts were obtained after treatment with Ar, H_2 and Ar/H_2, and the obtained samples were denoted as M-V_S/rGO (precursor containing thiourea) and M-V_O/rGO (precursor containing urea), where M = Ar, H_2 and Ar/H_2 (consistent with gas used to generate plasma).

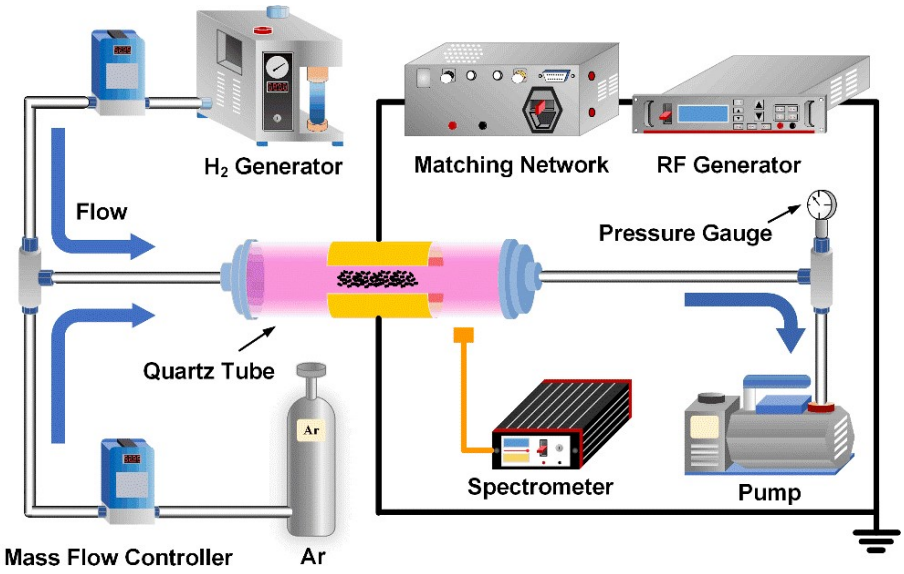

Fig. S1 Experimental platform for RF plasma-assisted treatment of materials.

3. Characterization

3.1 Microstructural characterizations

X-ray diffraction (XRD) data were acquired using a Bruker D8 ADVANCE diffractometer (Cu Kα, λ= 1.5406 Å). The diffraction patterns were recorded by continued scanning in the 2θ range of 5°–90° with an interval of 0.02°. Raman spectra were recorded on a Raman spectrometer (inVia, Renishaw PLC, UK) with 532 nm laser excitation. Transmission electron microscopic (TEM) and high-resolution transmission electron microscopic (HRTEM) images of the catalyst were obtained using a FEI Talos F200S G2 microscope. Scanning electron microscopy (SEM) images were performed with a Hitachi S-4800 scanning electron microanalyzer. X-ray photoelectron spectroscopy (XPS, Thermo ESCALAB 250 Xi) measurements were carried out using a monochromatic Al-Kα radiation source with an energy resolution of 0.1 eV to analyze the elemental composition of the catalyst as well as the chemical states of the surface elements and all the peak positions were charge-corrected with a C 1s spectrum at 284.8 eV. The Ocean USB2000+ spectrometer was used to collect emission spectra from 200 nm to 1100 nm during plasma treatment of the samples to define the active components during the discharge.

3.2 Electrochemical measurements

The M-V_S/rGO and M-V_O/rGO powders (5 mg) were dispersed by ultrasonication in a 1 mL mixed solution of ethanol and Nafion (5 wt%, DuPont) (v/v = 0.81:0.15) and

were used as the homogeneous ink. An appropriate amount of the ink was dropped onto a carbon cloth working electrode (1 cm × 1 cm). In addition, we also configured H_2-V_S/rGO and H_2-V_O/rGO as ink and dropped them on nickel foam (1 cm × 1 cm) as working electrodes, individually, and measured the OER performance and amperometric i-t curve test.

All the electrochemical measurements were performed on a CHI 760E electrochemical workstation using a typical three-electrode configuration. 1 M KOH has sued the electrolyte and the electrolyte was degassed by bubbling oxygen for at least 30 min prior to the electrochemical measurement to achieve a saturation condition of oxygen gas. An Ag/AgCl electrode was used as the reference electrode during the electrochemical measurements except for the amperometric i-t curve test in which HgO was used. A Pt foil was used as the counter electrode during the OER tests. Both the Ag/AgCl and HgO reference electrode s were calibrated before the OER measurements, and the calibration equations used were: $E_{RHE} = E_{Ag/AgCl} + 1.018$ V, in 1 M KOH and $E_{RHE} = E_{HgO} + 0.926$ V, in 1 M KOH, respectively Cyclic voltammetric (CV) measurements were carried out at a scan rate of 10 mV s^{-1}. Electrochemical impedance spectroscopic (EIS) measurements versus OER were carried out at different applied potentials in the frequency range of 10^{-2}-10^5 Hz. Amperometric i-t curve tests were performed for 12 h at a constant voltage of 1.6 V vs. RHE to test the current density of the samples. The OER activity of the catalyst was studied by linear sweep voltammetry (LSV) with a scan rate of 5 mV s^{-1} and in the potential range of 1-2 V vs. RHE. The

electrochemical active surface area (ECSA) of the materials was calculated by the double-layer capacitance (C_{dl}) method in order to explore the mechanism and improving the catalytic performance. The calculation of double-layer capacitance was based on the CV measurements at different scan rates (20, 40, 60, 80, 100, and 100 mV s^{-1}), and the region where no electrochemical reaction took place was selected as the electrochemical window.

4. DFT calculation

In this work, the energy and structure of each intermediate of CoS_2/rGO containing sulfur vacancies and Co_3O_4/rGO containing oxygen vacancies were calculated by first principle based density functional theory (DFT). The model systems of graphene-supported CoS_2 and Co_3O_4 nanoparticles were described as an optimized CoS_2 bulk and Co_3O_4 bulk supported on the (6 × 6) supercell graphene sheet. The substrates were adsorbed by cutting the (220) crystalline faces of CoS_2 and the (311) crystalline faces of Co_3O_4. DFT calculations were performed by DMol3, the Perdew-Burke-Ernzerhof (PBE) exchange-related generalized gradient approximation (GGA) was used in the calculations.

Figure

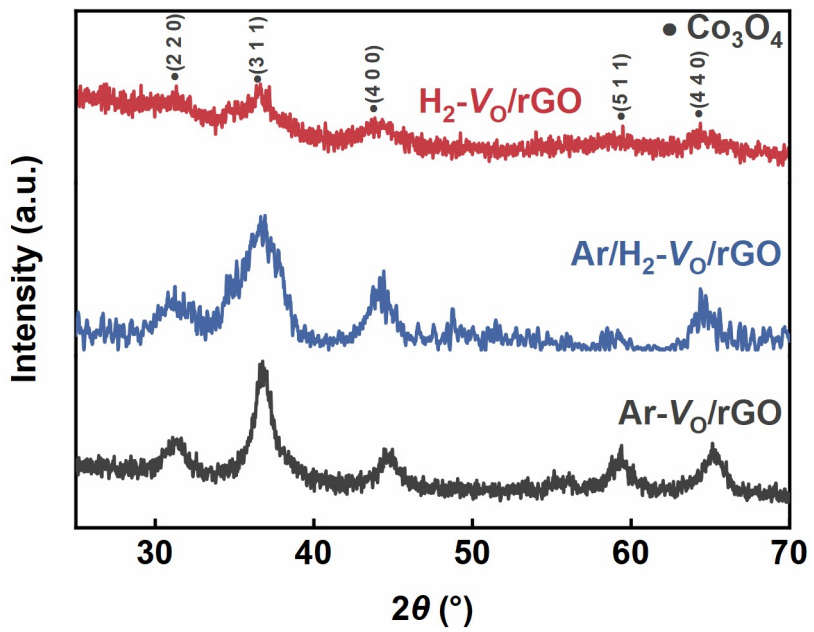

Fig. S2 XRD patterns of M-V_O/rGO (where M = H_2, Ar/H_2, Ar).

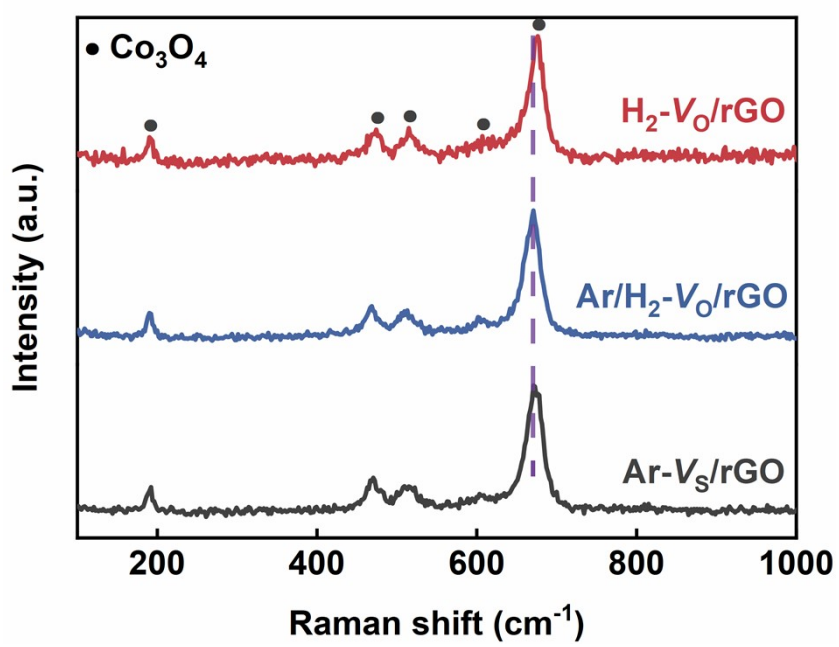

Fig. S3 Raman Spectrum of M-V_O/rGO (where M = H_2, Ar/H_2, Ar).

The strong peaks appearing for M-V_O/rGO near 188 cm^{-1}, 468 cm^{-1}, 510 cm^{-1}, and 667 cm^{-1} as shown in Fig. S3 can be attributed to Co_3O_4.[1,2] The blue shift of H_2-V_O/rGO relative to Ar/H_2-V_O/rGO and Ar-V_O/rGO indicates the presence of more oxygen vacancies in H_2-V_O/rGO.

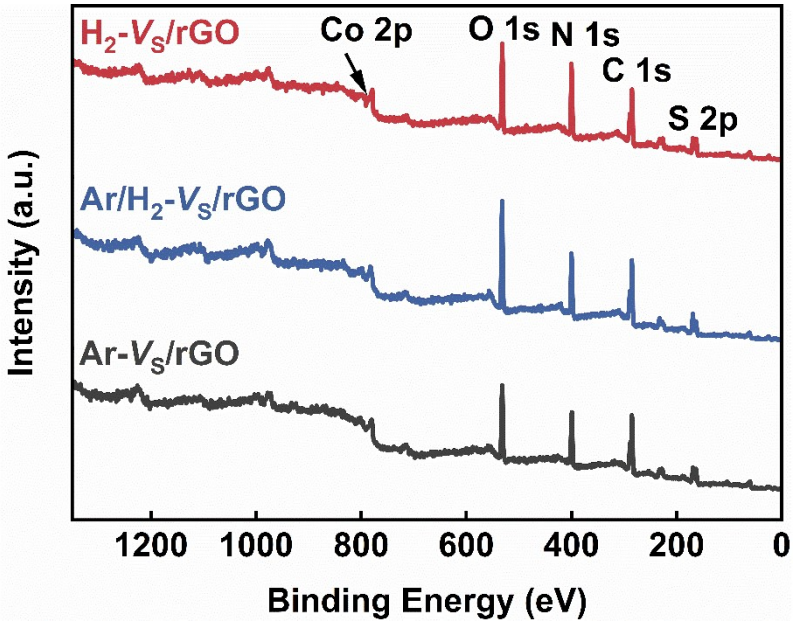

Fig. S4 XPS survey spectrum of M-V_S/rGO (M = H_2, Ar/H_2, Ar).

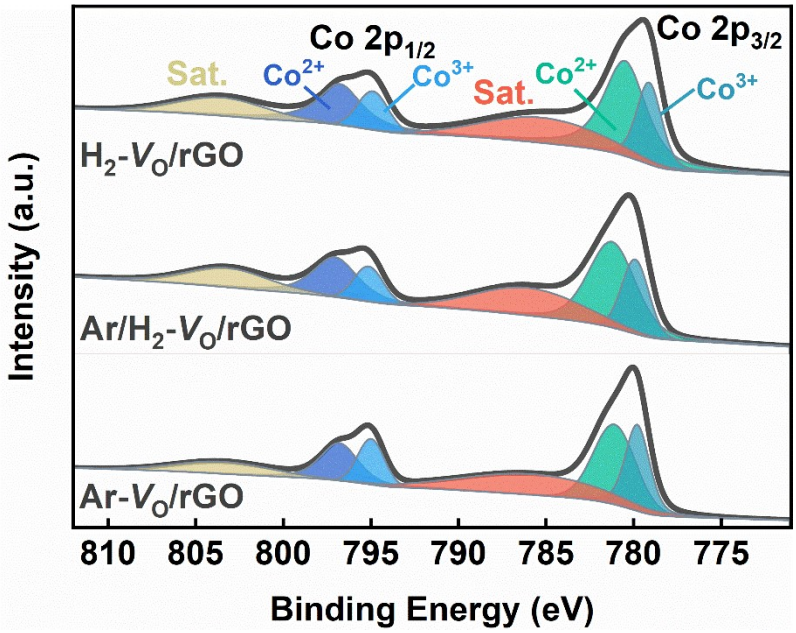

Fig. S5 Co 2p XPS spectrum of M-V_O/rGO (where M = H_2, Ar/H_2, Ar).

The main chemical form of Co loaded on the graphene surface is Co^{2+} (782 eV, 797.9 eV), and Co^{3+} (779.2 eV, 794.1 eV)[3,4] with the calculated Co^{2+}:Co^{3+} ratio for H_2-V_O/rGO, Ar/H_2-V_O/rGO and Ar-V_O/rGO being 2.23, 2.21 and 1.43, respectively, which indicates that more Co^{3+} is reduced to Co^{2+} in H_2-V_O/rGO and H_2 is more prominent in creating the oxygen vacancies.

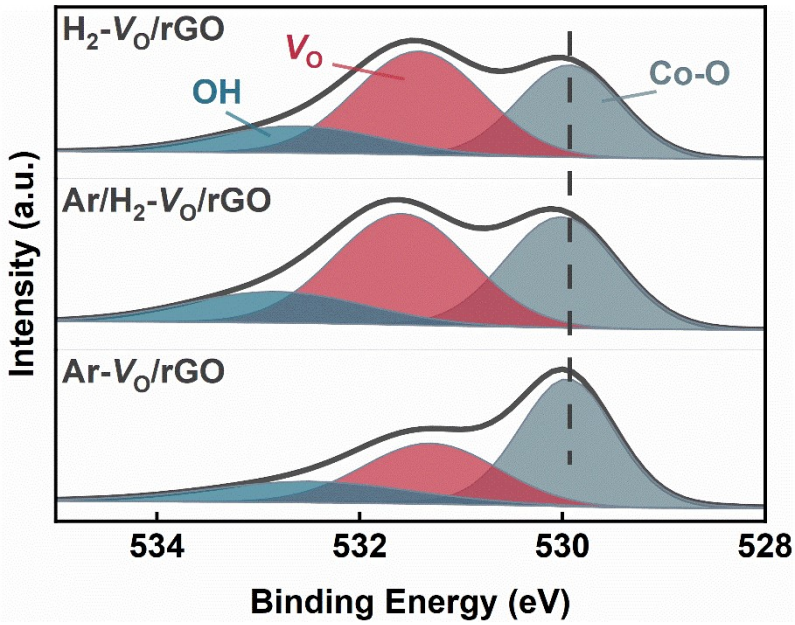

Fig. S6 O 1s spectrum of M-V_O/rGO (where M = H_2, Ar/H_2, Ar).

The binding energies of 529.8 eV, 532 eV, and 532.8 eV correspond to the characteristic peaks of Co-O, oxygen vacancies, and OH, respectively.[5] Among them, the Co-O characteristic peak was found to shift towards low binding energy with increasing H_2 concentration in the plasma, and the calculated percentage of V_O in the O 1s spectrum was 48.63% for H_2-V_O/rGO, 45.17% for Ar/H_2-V_O/rGO, and for Ar-

V_O/rGO it was 31.67%, thus clearly indicating more prominent ability of H_2 to create oxygen vacancies.

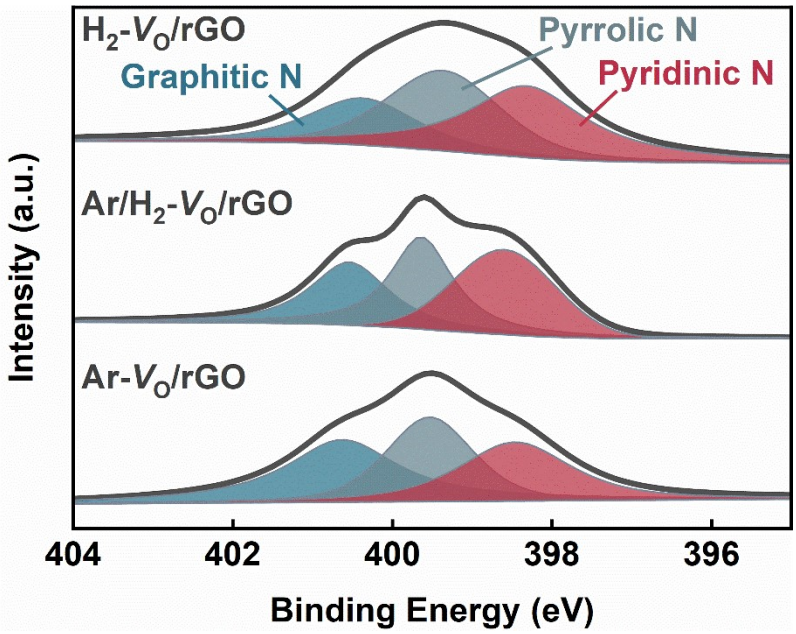

Fig. S7 N 1s spectrum of M-V_O/rGO (where M = H_2, Ar/H_2, Ar).

The binding energies of 398.3eV, 399.4eV, and 400.6 eV in the N 1s XPS spectrum of M-V_O/rGO correspond to the characteristic peaks of pyridine nitrogen, pyrrole nitrogen, and graphite nitrogen, respectively.[6-8] It has been shown that the presence of pyridine nitrogen is beneficial towards electrocatalytic performance.[9] The proportion of pyridine nitrogen in the N 1s spectrum was calculated to be 42.27%, 36.39% and 31.1% for H_2-V_O/rGO, Ar/H_2-V_O/rGO, and Ar-V_O/rGO, respectively, which also explains the more excellent electrocatalytic performance of H_2-V_O/rGO.

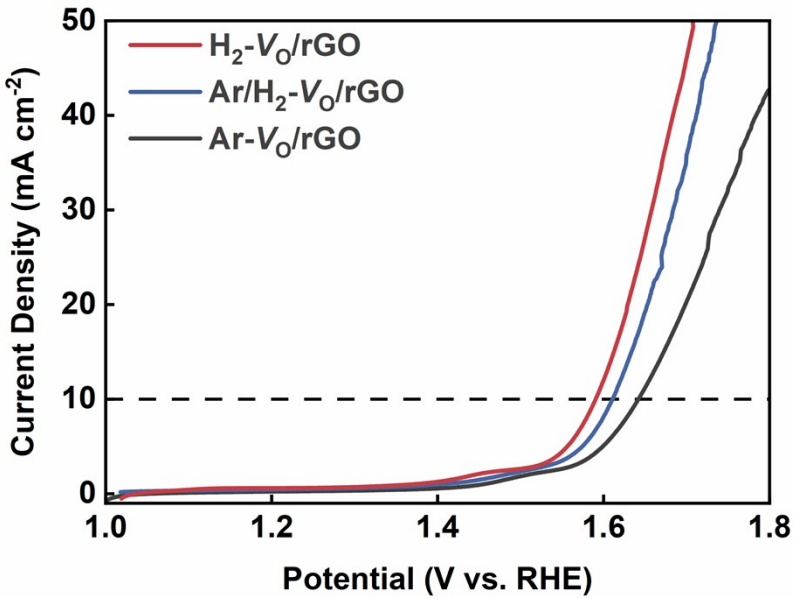

Fig. S8 LSV curve of M-V_O/rGO (where M = H_2, Ar/H_2, Ar).

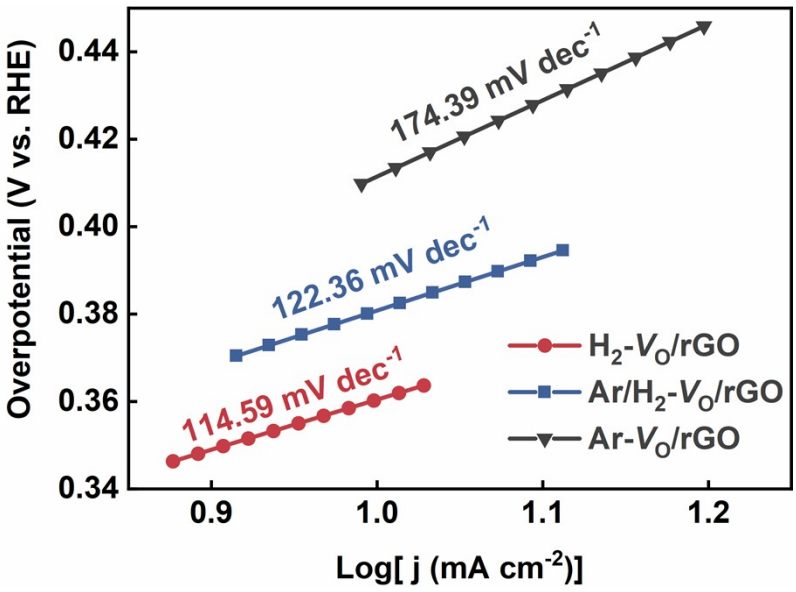

Fig. S9 Tafel slope of M-V_O/rGO (where M = H_2, Ar/H_2, Ar).

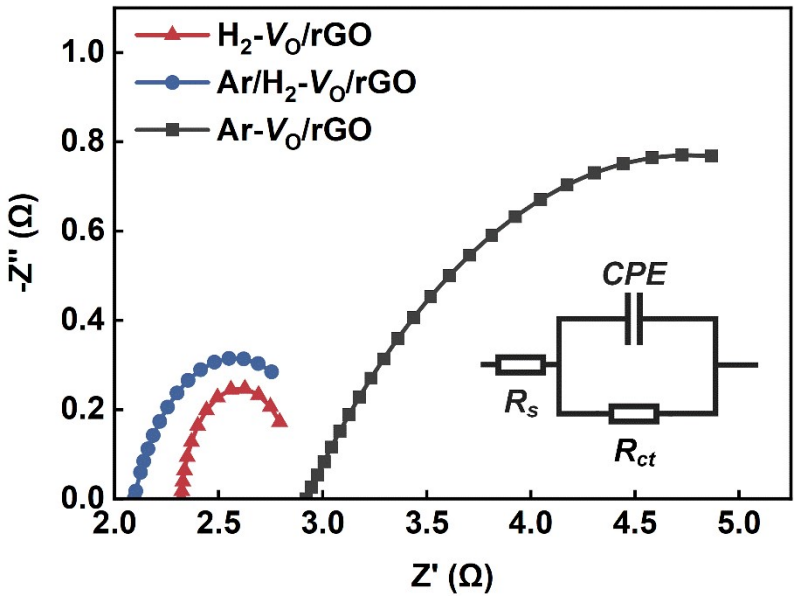

Fig. S10 Nyquist plots of M-V_O/rGO (where M=H_2, Ar/H_2, Ar).

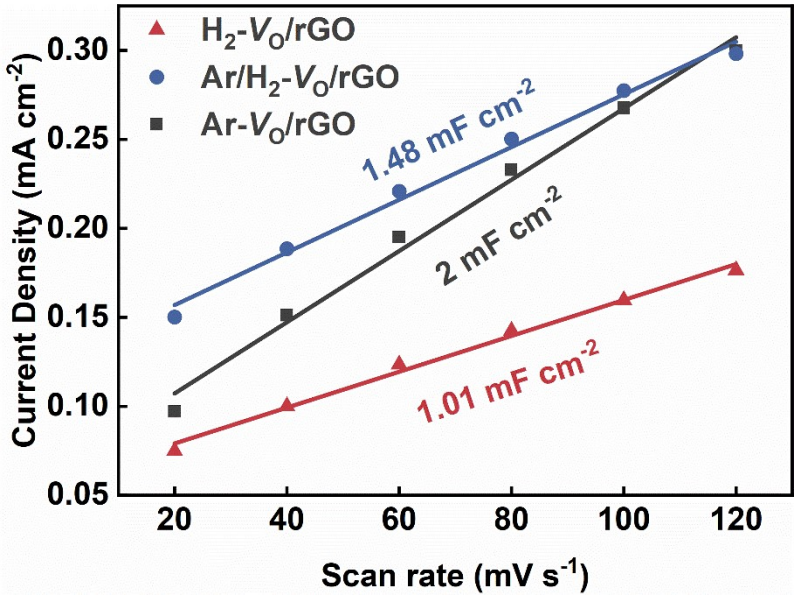

Fig. S11 Capacitive current density against scan rates of M-V_O/rGO (where M = H_2, Ar/H_2, Ar).

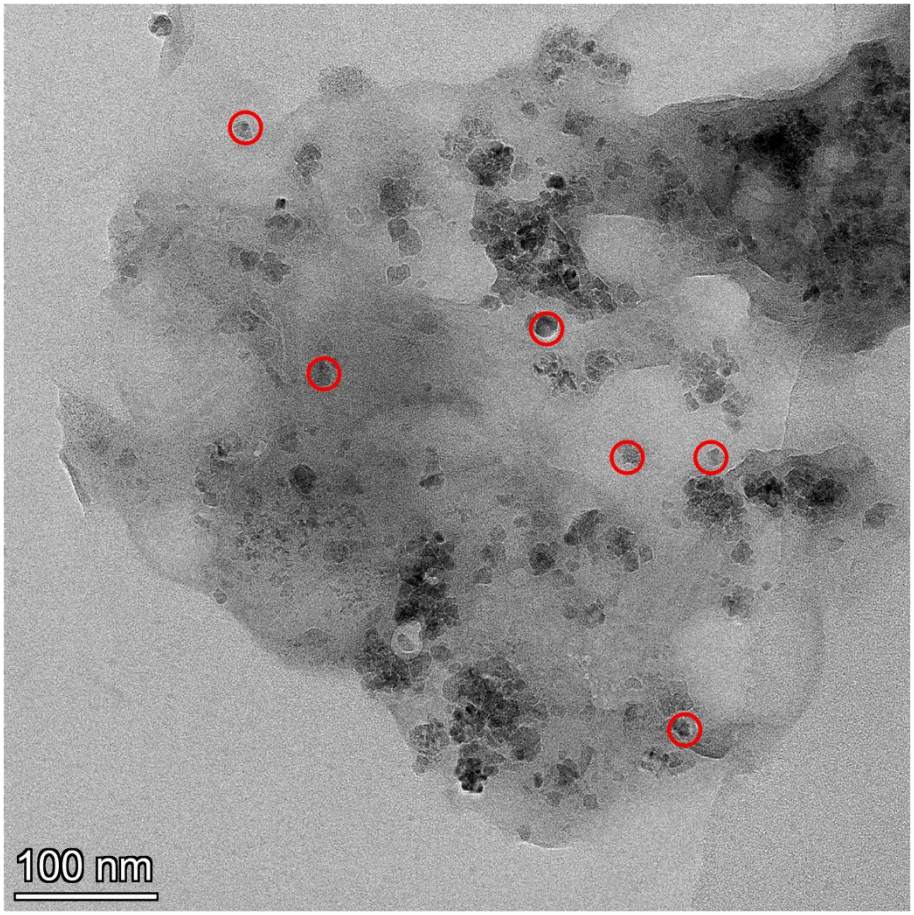

Fig. S12 TEM of Ar-V_S/rGO, red circles denote nanopores on the rGO surface.

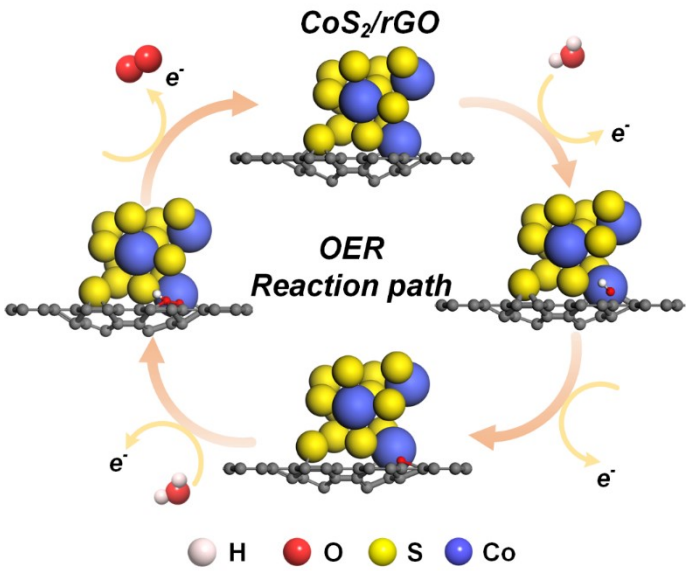

Fig. S13 Schematic illustration of the OER pathway.

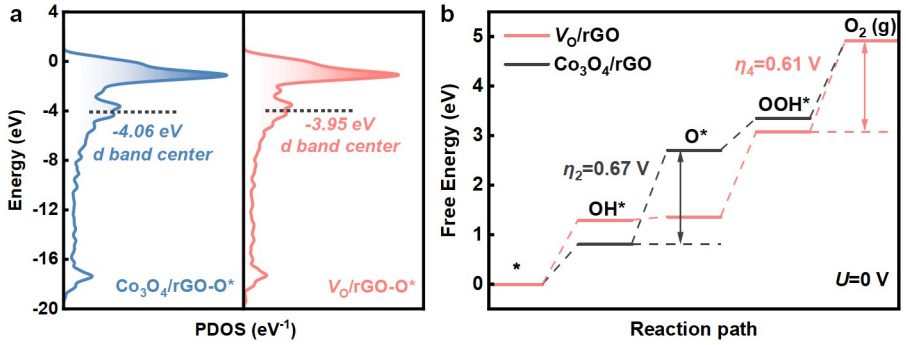

Fig. S14 (a) Partial density of states (PDOS), (b) OER free-energy diagram.

For comparative DFT calculations between V_O/rGO and Co_3O_4/rGO, we used the (331) crystal plane of Co_3O_4 as the subject of our study. Fig. S14a shows the calculated partial density of states (PDOS) for V_O/rGO-O*and Co_3O_4/rGO-O*. Compared to Co_3O_4/rGO-O*, center of the active electron density band (d energy band) of V_O/rGO-O* shifted toward the vacuum layer. The corresponding free energy diagram (Fig. S14b) shows a significantly lower energy barrier for O* formation on the surface of V_O/rGO (ΔG_2) compared to that of Co_3O_4/rGO. And the presence of oxygen vacancies results in the occupation of the vacancies created by the original O atoms by the catalyst during adsorption of O to form a stable structure. It indicates that the introduction of oxygen vacancies enhances the binding strength for the adsorption of substrate molecules in Co_3O_4/rGO, which is favorable for the OER process. The ΔG_4 is significantly higher for the surface of V_O/rGO compared to that of Co_3O_4/rGO. It indicates that the V_O/rGO is less able to desorb O_2 and the RDS shifts from the second step to the fourth step, thus reducing the overpotential of the reaction.

References

1 M. Rashad, M. Ruesing, G. Berth, K. Lischka and A. Pawlis, CuO and Co3O4 Nanoparticles: Synthesis, Characterizations, and Raman Spectroscopy, *J. Nanomater.*, 2013, **2013**, 714853.

2 S. Deng, N. Chen, D. Deng, Y. Li, X. Xing and Y. Wang, Meso- and macroporous coral-like Co3O4 for VOCs gas sensor, *Ceram. Int.*, 2015, **41**, 11004–11012.

3 L. Liu, Z. Jiang, L. Fang, H. Xu, H. Zhang, X. Gu and Y. Wang, Probing the Crystal Plane Effect of Co3O4 for Enhanced Electrocatalytic Performance toward Efficient Overall Water Splitting, *ACS Appl. Mater. Interfaces*, 2017, **9**, 27736–27744.

4 M. Kuang, T.T. Li, H. Chen, S.M. Zhang, L.L. Zhang and Y.X. Zhang, Hierarchical Cu2O/CuO/Co3O4 core-shell nanowires: synthesis and electrochemical properties, *Nanotechnology*, 2015, **26**, 304002.

5 D. Liu, C. Zhang, Y. Yu, Y. Shi, Y. Yu, Z. Niu and B. Zhang, Hydrogen evolution activity enhancement by tuning the oxygen vacancies in self-supported mesoporous spinel oxide nanowire arrays, *Nano Res.*, 2018, **11**, 603–613.

6 X. Zhang, Q. Fan, N. Qu, H. Yang, M. Wang, A. Liu and J. Yang, Ultrathin 2D nitrogen-doped carbon nanosheets for high performance supercapacitors: Insight into the effects of graphene oxides, *Nanoscale*, 2019, **11**, 8588–8596.

7 J. Zhang, J. Chen, Y. Luo, Y. Chen, X. Wei, G. Wang and R. Wang, Sandwich-like electrode with tungsten nitride nanosheets decorated with carbon dots as efficient electrocatalyst for oxygen reduction, *Appl. Surf. Sci.*, 2019, **466**, 911–919.

8 X. Zhang, P. Yang and S.P. Jiang, The edge-epitaxial growth of yellow g-C3N4 on red g-C3N4 nanosheets with superior photocatalytic activities, *Chem. Commun.*, 2021, **57**, 3119–3122.

9 Y. Zhu, T. Zhang and J.Y. Lee, Nitrogenated-Graphite-Encapsulated Carbon Black as a Metal-Free Electrocatalyst for the Oxygen Evolution Reaction in Acid, *ChemElectroChem*, 2018, **5**, 583–588.